

# Measurement-based hydrodynamic characterisation of reed – open water interface zones in shallow lake environment

Melinda Kiss / János Józsa

Received 2013-12-12, revised 2014-05-21, accepted 2014-06-12

## Abstract

Gradient-driven interactions and exchange mechanisms of the reed – open water interface in shallow lake environment were investigated by localised field measurements and detailed data analysis. High frequency 3D flow velocities were recorded in several points throughout a typical interface zone of Lake Fertő. Based on the data the flow distribution, specific discharge, energy dissipation rate, turbulent characteristics, sediment deposition and resuspension tendencies were quantified near and inside the reed zone. Moving toward and into the reed zone, the decrease of the mean velocity component perpendicular to the interface, velocity fluctuation and the wave-related energy content of the flow were revealed along with the increasing tendency of the energy dissipation rate. Investigating the effect of different decomposition techniques on the turbulent characteristics, the one enabling the decomposition of wave-related components from turbulent components was suggested. Finally, continuous sediment deposition and the lack of resuspension were estimated in the investigated area.

## Keywords

Shallow lake · reed – open water interface · exchange flow · energy dissipation rate · turbulent characteristics · sediment deposition and resuspension

## Melinda Kiss

Budapest University of Technology and Economics, Department of Hydraulic and Water Resources Engineering also MTA-BME Water Management Research Group, Műegyetem rkp. 3, H-1111 Budapest, Hungary  
e-mail: kiss.melinda@epito.bme.hu

## János Józsa

Budapest University of Technology and Economics, Department of Hydraulic and Water Resources Engineering also MTA-BME Water Management Research Group, Műegyetem rkp. 3, H-1111 Budapest, Hungary

## 1 Introduction

Emergent aquatic plants often grow in shallow lakes in form of patches or larger extended regions in the littoral zones. One of their most common types in Europe is the reed (*Phragmites australis*). These canopies usually play an important role in the fate of the given water body regarding both the physical and ecological (often called abiotic and biotic) processes. Water exchange across the reed – open water interface have a great influence on the flushing, but at the same time sedimentation of the reed zone and transporting oxygen, phosphorus and other substances between the two zones [6]. The mixing of the two water bodies possessing different physical properties contributes to the relatively fresh water supply of reed zone from open water areas resulting in an improved status of the vegetation in the long term. A canopy in such a good status provides then a vital source of habitat and food for zooplankton, invertebrates, fish and for many bird species, thus, they enhance the biodiversity of the lake [4].

As an additional physical process, dense canopy with its enhanced drag due to the plant stems cause wave damping resulting in deposition from the entering, usually sediment-laden water bodies [8]. In the pelagic zones of shallow lakes, resuspension has got a great influence on lake ecosystem. It causes not only light attenuation thus affecting the growth of submerged plants, but also assists the increase of phytoplankton mass due to its potential to release nutrients into the water column [13]. Within aquatic plants, the resuspension potential significantly decreases with the decreasing flow velocity and turbulent energy content and thus with the reduced near-bed stresses. According to [13], the resuspension rate within emergent plants was on average 43% of that in the adjacent open water and the internal phosphorus loading decreased with 26 mg/m<sup>2</sup>/day within the canopy.

Since littoral lake zones covered with aquatic vegetation differ from the pelagic ones in a number of characteristics, various gradient-driven interaction and exchange mechanisms take place at the littoral-pelagic interface strongly affecting both zones and thus the whole lake.

As was presented in [11], extended reed zones affect the spa-

tial distribution of the over-lake wind field in a complex way. Relatively large roughness height characterising the windward reed zone was found to turn up above open water at short pelagic fetch indicating that wind conserves its preceding equilibrium profile for a given short distance downwind of the reed canopy and at longer fetch it quickly transforms into a new profile fitting the open water. It was also shown that the near-canopy wind profile might deviate from the widely used theoretical logarithmic form. Considering the wind profile parameters of distinct thermal stability classes, it was concluded that the length of sheltered zone behind the canopy and the rate of the IBL development depend on thermal stratification, namely in unstable conditions the profile realignment takes place closer to the reed zone. In addition, abrupt change of the horizontal wind speed at the anemometer height of 5.3 m was detected at about 35 m pelagic fetch, clearly indicating the border of the developing internal boundary layer (IBL).

The basis of the developing lake currents and water exchange processes at the reed – open water interface is the near-canopy wind field since these water motions are predominantly wind-driven. Therefore, the spatially and temporally varying near-canopy wind field might generate complex lake flow conditions in the immediate vicinity of the reed zone. In addition, the presence of reed canopy itself modifies the spatial distribution of wind-driven lake currents due to the drag exerted by reed stems. However, as the exchange mechanisms are controlled primarily by the near-canopy flow conditions, the exploration of this quite complex flow field near and inside the canopy has got great importance.

Simultaneous wind speed and lake flow velocity measurements were conducted in Lake Fertő in several measurement campaigns in 2012 and 2013. The present study attempts to reveal the gradient-driven interactions and exchange mechanisms of the reed – open water interface through the investigation of the flow field, specific discharge, energy dissipation rate, turbulent characteristics and sediment deposition as well as resuspension tendency near and inside the reed zone.

## 2 Field conditions and data acquisition

Lake Fertő (Neusiedler See in German) located at the Hungarian-Austrian border was chosen as case study because of its extended reed cover and extreme shallowness. It has a surface area of 315 km<sup>2</sup>, out of which 180 km<sup>2</sup> is covered by reed [17] not just along the shoreline as a belt but also in patches in various scale, especially on the Hungarian side. The average depth of the pelagic zone is not more than 1.5 m at long term average water surface elevation, while the water depth in the reed zones is just a few tens of centimetres even in high water surface elevation. However, by low water conditions, which happened for example in 2012, large part of the reed zones dried out for the summer period. The primarily chosen measurement site is characterised by a sharp transition between reed canopy and open water, quite a typical location to the lake. The average canopy

height of the investigated area was about 3.4 m; the vegetation density was around 230 stem/m<sup>2</sup> right at the reed border where the environmental conditions enable the growth of vegetation and 120 stem/m<sup>2</sup> inside the canopy. The stem diameter at the water surface was 8-10 mm. As an overall characterisation of the aerodynamic exposure of Lake Fertő and its surroundings, the two prevailing wind directions are NNW and SSE, which was experienced also during the measurement campaigns.

Fig. 1 shows the location of the wind and lake flow measurements on an orthophoto of the area taken in 2007. It also indicates the extension of reed zone (thick line) according to the latest survey conducted in 2012. Wind measurement was done with a 3-dimensional CSAT3 sonic anemometer placed inside the reed zone about 15 m from the reed borderline. The sensor height was 5.3 m above the water surface elevation observed at the time of deployment. Continuous 10 Hz recording was accomplished during the investigation period.

3D acoustic Doppler velocimeters (ADV) were used to reveal the flow conditions of the reed – open water interface zone. The applied type of ADV, the Nortek Vectrino Lab Probe was designed for laboratory conditions, thus its small dimensions and suitable form enabled its application even in low water depth and also between the rather densely standing reed stems, both huge limitations for such measurements. Flow velocities were revealed at 25 Hz sampling frequency with two synchronized ADVs, their synchronization was made by means of PolySync software. Fixing one of the instruments in a reference point and moving the other one in ten-minutes periods along an axis locally nearly perpendicular to the reed borderline, high frequency 3D velocities were recorded at several points in multiple depths from 12 m inside the canopy to 16 m outside.

## 3 Data analysis methods

### 3.1 Spike filtering and coordinate rotation

Since high sampling rate (25 Hz) was used in the ADV measurements and very low flow velocities occurred already at a few metres inside the reed canopy, the instruments recorded at places and times erroneous data. These so-called spikes in the time series were numerically removed by the Velocity-Correlation Filter technique [3].

To evaluate the water exchange through the interface of reed and open water zones, the original velocities measured in East-North-Up (ENU) framework had to be rotated to get velocity components directing into the reed. Multiplying the original components ( $u_{or}$  and  $v_{or}$ ) by  $R(\theta)$  rotation matrix, the new components, perpendicular ( $u$ ) and parallel ( $v$ ) to the reed borderline, are the following:

$$\begin{bmatrix} u \\ v \end{bmatrix} = R(\theta) \cdot \begin{bmatrix} u_{or} \\ v_{or} \end{bmatrix} = \begin{bmatrix} \cos \theta & -\sin \theta \\ \sin \theta & \cos \theta \end{bmatrix} \cdot \begin{bmatrix} u_{or} \\ v_{or} \end{bmatrix}, \quad (1)$$

where  $\theta$  is the rotation angle.

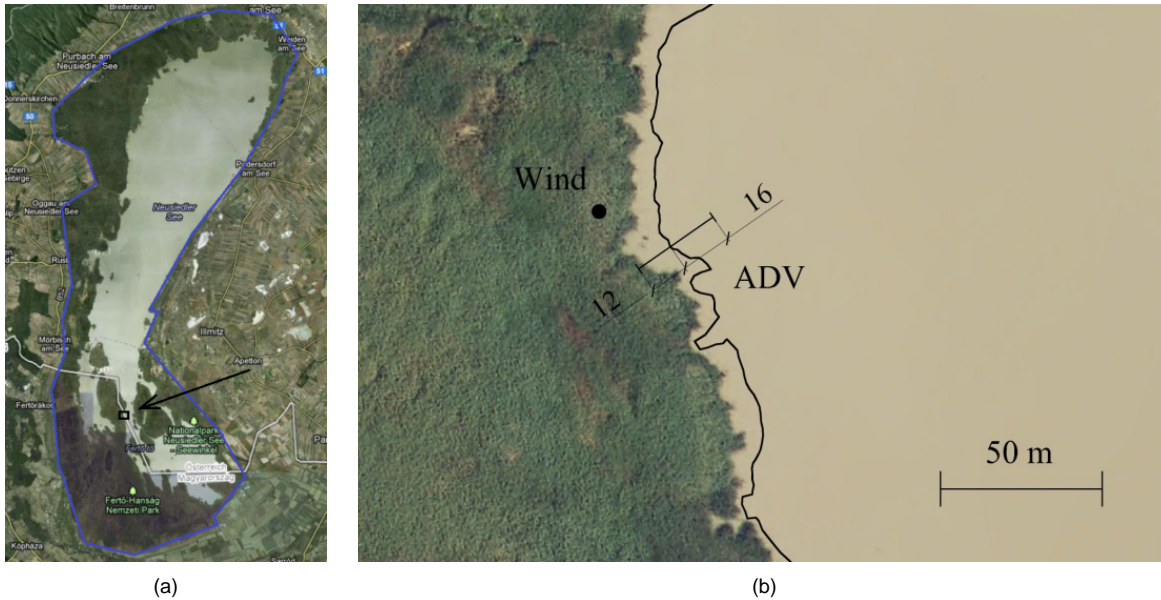


**Fig. 1.** Measurement locations: (a) Orthophoto taken in 2007 on Lake Fertő and the measurement area indicated by a square. (b) Wind measurement loca-

tion and the axis along which ADV measurements were conducted. Thick line denotes the reed borderline according to the latest survey in 2012

### 3.2 Time series analysis

To investigate how the presence of the dense canopy alters the lake flow velocities moving further and further inside the canopy, the velocity time series measured at different points were compared to each other by means of time-series analysis. According to a relevant handbook [5] providing wide collection of data analysis methods, the mean, standard deviation, autocorrelation function and spectral analysis of each time series were derived.

First, Reynolds decomposition was applied to estimate the turbulent fluctuation of velocity components ( $u'$ ,  $v'$  and  $w'$ ):

$$\begin{aligned} u(t) &= \bar{u} + u'(t) \\ v(t) &= \bar{v} + v'(t) \\ w(t) &= \bar{w} + w'(t) \end{aligned} \quad (2)$$

where  $u(t)$ ,  $v(t)$ , and  $w(t)$  are the instantaneous conventional orthogonal velocity components,

$\bar{u}$ ,  $\bar{v}$  and  $\bar{w}$  are the Reynolds-averaged mean velocities and  $u'(t)$ ,  $v'(t)$  and  $w'(t)$  are the instantaneous fluctuation around the mean.

Reynolds decomposition can be only applied if the flow is in steady or at least in quasi steady state meaning that its changes are slow enough not to observe in the recording interval. Therefore, short, 10-minutes measurements were conducted at each investigated point and only time series fulfilling the criterion of the quasi steady state were considered in further analysis.

According to an additional criterion regarding the turbulent data analysis, the flow data have to be also in statistically stationary state. Thus, the dependence of statistics on the length of the time series has to be first investigated with cumulative tests.

Cumulative average provides the average of the velocity components versus the duration of the averaging. It shows an initial transient period ( $T^*$ ) with low sample size, where the average has a high variation, whereas after this period with increasing sample size and recorded period components, the average converges to a unique value indicating that the data series reach a statistically stationary state. Consequently, if the measurement length is longer than this transient period, the statistics become independent of the measurement length or their changes are negligibly small [18]. The recorded 10-minutes long data series proved sufficient for turbulent data analysis, verified by means of cumulative mean and cumulative variance test.

For the perpendicular ( $u$ ) velocity component, the mean value and variance can be estimated by

$$\bar{u} = \frac{1}{N} \sum_{i=1}^N u(t_i) \quad \wedge \quad \sigma^2 = \frac{1}{N} \sum_{i=1}^N [u(t_i) - \bar{u}]^2, \quad (3)$$

respectively, where  $N$  is the sample size and  $t_i$  ( $i = 1, 2, \dots, N$ ) are the discrete times of measurements.

Mean and variance can be analogously expressed for the other two components,  $v$  and  $w$ . The standard deviation ( $\sigma$ ) is then the square root of the variance.

The strength of the correlation between two datasets can be characterised with covariance and correlation functions. The autocovariance function is based on shifted correlation of the fluctuation time series with itself:

$$\varphi_{uu}(s) = u'(t) \cdot \bar{u}'(t+s) = \frac{1}{N-k} \sum_{i=1}^{N-k} u'_i \cdot u'_{i+k} \quad (4)$$

where  $s = k \cdot \Delta t$  is the time lag for  $k$  sampling time increments.

For autocorrelation function, there are two approaches, both widely used by hydraulic engineers and oceanographers [5]. Ac-

cording to the first, correlation function can be estimated analogous to covariance function but it applies raw data series before removal of the mean instead of fluctuation time series. However, according to the second approach, which was chosen in the present research, the correlation function can be gained by normalizing the covariance function with the variance:

$$\rho_{uu}(s) = \frac{\varphi_{uu}(k \cdot \Delta t)}{\sigma_{uu}^2} = \frac{1}{\bar{u}_i^2} \frac{1}{N-k} \sum_{i=1}^{N-k} u'_i \cdot u'_{i+k} \quad (5)$$

The autocorrelation function shows the degree of correlation between the original and shifted time series changing with increasing time lag. Because of the normalization, its values are between 1 and -1. If there is periodicity in the time series, the autocorrelation function provides high values at time lags corresponding to the period.

To investigate the most dominating frequencies in a time series and the distribution of turbulent kinetic energy between the different frequencies, spectral analysis was conducted. The power spectral density can be derived from autocovariance function by means of Fast Fourier Transformation (FFT). For discrete time series it is written as follows:

$$S_u(f) = \frac{2}{\pi} \sum \varphi_{uu}(t) \cdot \cos(2\pi \cdot f \cdot t) \quad (6)$$

### 3.3 Energy dissipation

According to [20], the turbulent kinetic energy budget can be assumed as a balance between shear production ( $P$ ) and energy dissipation ( $E$ ). In the inertial subrange of power spectral density the larger scale flow structures with energy-producing lower frequencies transform into smaller scale eddies with energy-dissipating high frequencies, which is called energy cascading.

Assuming local isotropy and stationarity of the turbulence, the power spectral density in the inertial subrange can be expressed as:

$$F_i(k) = \alpha_i \varepsilon^{2/3} k^{-5/3} \quad (7)$$

where  $F_i(k)$  is the spectral density of the  $i^{\text{th}}$  velocity component,

$k$  is the wave number,

$\varepsilon$  is the mean energy dissipation rate and

$\alpha_i$  is the one-dimensional Kolmogorov constant. In locally isotropic turbulence  $\alpha_1 \sim 0.51$  and  $\alpha_2 = \alpha_3 \sim 0.69$ , as found e.g. in [10].

The power spectral density in the frequency domain  $S(f)$  can be related to that in the wave number domain by means of the Taylor "frozen turbulence" hypothesis, where  $k = 2\pi f / \bar{u}_i$ :

$$S_i(f) = \frac{2\pi}{\bar{u}_i} F_i(k) \quad (8)$$

From Eq. (7) and Eq. (8), the dissipation rate can be estimated

as follows:

$$\varepsilon = \frac{2\pi}{\bar{u}_i} \left( \frac{f^{5/3} S_i(f)}{\alpha_i} \right)^{3/2} \quad (9)$$

An other theoretical approach was defined by [20] to express the energy dissipation rate. According to this, the rate of energy transfer from large to small scales is determined by the energy of the large eddies and their time scale, which are in the order of  $U^2$  and  $L/U$ , respectively. Thus, the dissipation rate can be given as

$$\varepsilon = AU^3/L \quad (10)$$

This relation is valid if there exists only one characteristic length  $L$ . In the expression,  $U$  is the characteristic velocity scale and  $A$  is an undetermined constant in the order of one.

### 3.4 Turbulent characteristics

In order to better understand the effect of reed canopy on currents, Reynolds number, turbulent kinetic energy ( $TKE$ ), bottom shear stress, friction velocity and turbulent intensity were estimated at each measurement point. These parameters describe the driving factors for resuspension and deposition of sediment and the near-bed structure of turbulence [10]. Reynolds number ( $Re = UL/\nu$ ) was calculated using the mean horizontal velocity as characteristic velocity scale ( $U$ ) and the water depth as the characteristic length scale ( $L$ );  $\nu$  is the kinematic viscosity. While in open-channel flows bed- and wind-generated turbulence dominates, in the reed zone turbulence is generated mainly by plant stems causing vortex shedding. Therefore, inside the canopy the average stem diameter ( $d$ ) should be applied as characteristic length scale [9]. Reynolds number based on  $d$  as length scale will be denoted as  $Re_d$ .

Turbulent kinetic energy was estimated from the velocity fluctuation with the widely used formula

$$TKE = (u'^2 + v'^2 + w'^2) / 2 \quad (11)$$

According to [19], the following simple linear relationship exists between turbulent energy and shear stress:

$$\tau = C_1 \cdot TKE, \quad (12)$$

where  $C_1$  – proportionality constant ( $\sim 0.2$ , see e.g. [19]).

The friction velocity  $u_{b_s}$  at the lake bottom can be then determined as

$$u_{b_s} = \sqrt{\frac{\tau}{\rho}}, \quad (13)$$

where  $\rho$  – density of the water.

An other often used measure of the turbulence is the turbulence intensity ( $TI$ ) expressed as

$$TI = \frac{\sqrt{TKE}}{\bar{u}} \quad (14)$$

## 4 Results

### 4.1 Flow velocities in the interface zone

Lake flow measurements conducted at several points of an axis locally perpendicular to the reed border allow observing the spatial variation of flow features at the interface of the reed and open water zones. After spike filtering and coordinate rotation applied on the raw data sets according to Chapter 3.1, a reed border-aligned coordinate system was defined with velocity components perpendicular ( $u$ ) and parallel ( $v$ ) to the reed border and with the unchanged  $w$  vertical velocity component.

Table 1 summarizes the Reynolds averaged mean and fluctuation term of the three components at several measurement points along with the main wind features characterising the time interval of the given flow measurement. Positive  $u$  points toward the reed (close to the West) and positive  $v$  points close to the South. In the first column 0 m denotes the location of the reed border, positive values refer to distances inside the canopy while negative ones to locations out of it. Relative depth is given by the ratio of measurement depth and total water depth. Generally, the decrease of mean velocity and mean absolute fluctuation of all three velocity components were detected moving toward and into the canopy and approaching the bottom. Perpendicular velocity components directing toward the reed at -8 m at both measurement depths indicate that wind-driven flow approaches the reed zone, while moving into the canopy mean flow velocity decreases rapidly due to the enhanced drag of dense vegetation. At some locations mean perpendicular velocity is negative indicating a developed return flow within the canopy. The occasional diverse directions of flow velocities at two points of the same vertical suggest that near and within the canopy 3D description of the flow structure is needed. Fig. 2 shows the spatial and temporal variation of near-canopy currents by displaying the time series of the instantaneous perpendicular velocity components of four outer measurement points, namely at -8 and 0 m in both depths. The reduction of mean perpendicular velocity and velocity fluctuation can also be observed here moving toward the vegetation and toward the lake bottom.

To account for unsteady conditions occurring during the whole investigation period, the one-second averages of each velocity component were normalized with the ones of the reference point placed at the reed border at 0 m. The exponential reduction of normalized velocity components can be observed moving towards and into the reed zone (Fig. 3 and Table 2). Normalized perpendicular ( $u$ ) and parallel ( $v$ ) velocity components at 8 m are 60 and 12 times larger than the ones at the reed border. Moving further inside the canopy the decrease of  $u$  and  $v$  velocity components is not that much rapid any longer; furthermore, perpendicular velocities might change their sign at some inner locations and direct toward the open water which is in agreement with Table 1.

### 4.2 Specific discharge across the interface zone

The specific discharge ( $q$ ) across the reed – open water interface can be calculated multiplying the perpendicular velocity and the water depth. Flow measurement was conducted in two depths of about 25% and 75% of the total water depth, and an assumption was made that velocity measured at the upper point characterises well the upper half of the vertical while the velocity of the lower measurement point characterises the lower half of the vertical. Therefore, the specific discharge of the whole vertical could be estimated as the mean of the specific discharges at these two points. This is a more sufficient way of discharge calculation than considering only a single point measurement of the vertical, especially under weak wind or calm conditions when thermally driven exchange flow can become important with a complex vertical velocity profile as suggested by [22]. Fig. 3 includes the mean specific discharge versus the position relative to the reed border with a second vertical axis, showing the exponential decrease of  $q$  when moving toward and into the reed zone. According to the calculations, the mean  $q$  right at the reed border was  $1.4 \text{ m}^3/\text{hour}/\text{m}$  during the measurement, while the mean incoming  $q$  and mean outgoing  $q$  were  $17.2 \text{ m}^3/\text{hour}/\text{m}$  and  $15.6 \text{ m}^3/\text{hour}/\text{m}$ , respectively (Table 2).

Specific discharge provides information not only about the rate of water exchange but also the transport of substances such as dissolved oxygen, phosphorus or even suspended sediment particles across the reed – open water interface since transport of a given substance can be estimated as the product of its concentration and the specific discharge. An example of sediment deposition estimation from  $q$  will be given in Chapter 4.6.

### 4.3 The wave damping effect of the canopy

Mean vertical velocities providing information about the waves were in general one order of magnitude lower than the horizontal ones in the investigation periods and show a decrease with increasing distance inside the canopy (Table 1). The damping of waves is expected to occur when the flow enters the reed zone possessing enhanced drag due to the densely populated plant stems. Plotting together the autocorrelation functions of the vertical component of 3 measurement points lying in different distances from the reed border, the magnitude of wave damping can be expressed (Fig. 4). The autocorrelation function of  $w$  at time lags corresponding to the period is high at 8 m out of the reed zone and right at the reed border, thus the time series measured here correlate well with their previous state. However, this correlation is significantly lower already at 8 m inside the canopy. The period, which is the time difference between two consecutive downcrossings, is about 1.3, 1.1 and 1.3 s, respectively.

Identical periods can be detected from the power density spectra generated from the vertical velocity data of the same three points (Fig. 5) since, as is known, the period is the reciprocal of the frequency belonging to the spectral peak. The plot indicates that flow energy in the wave-related range of the spectra is

**Tab. 1.** Reynolds averaged mean and fluctuation of the three velocity components near and inside the reed canopy with the corresponding wind features.

distance		relative depth	wind speed	wind direction	$\bar{u}$	$ \overline{u'} $	$\bar{v}$	$ \overline{v'} $	$\bar{w}$	$ \overline{w'} $
from reed border	m									
-8	0.32	2.4	SE	<b>1.56</b>	3.94	<b>-2.15</b>	3.07	<b>0.11</b>	3.47	
-8	0.88	2.7	SE	<b>1.02</b>	1.49	<b>-1.63</b>	1.18	<b>0.23</b>	0.50	
-4	0.26	1.3	NE	<b>-0.09</b>	1.16	<b>0.81</b>	1.86	<b>-0.06</b>	0.51	
-4	0.71	0.7	N	<b>0.74</b>	0.97	<b>0.28</b>	1.68	<b>-0.05</b>	0.30	
0	0.29	2.3	SE	<b>0.15</b>	2.34	<b>-0.51</b>	3.30	<b>-0.09</b>	2.49	
0	0.86	2.1	SE	<b>-0.04</b>	0.99	<b>-0.02</b>	1.37	<b>-0.13</b>	0.50	
2	0.31	1.5	N	<b>-0.12</b>	1.03	<b>0.16</b>	1.94	<b>-0.10</b>	0.90	
2	0.74	1.6	NE	<b>0.25</b>	0.92	<b>0.16</b>	1.77	<b>-0.09</b>	0.55	
8	0.36	1.5	N	<b>-0.10</b>	1.16	<b>-0.01</b>	1.05	<b>-0.07</b>	0.38	
8	0.74	1.1	N	<b>0.16</b>	0.96	<b>0.01</b>	1.00	<b>-0.03</b>	0.41	

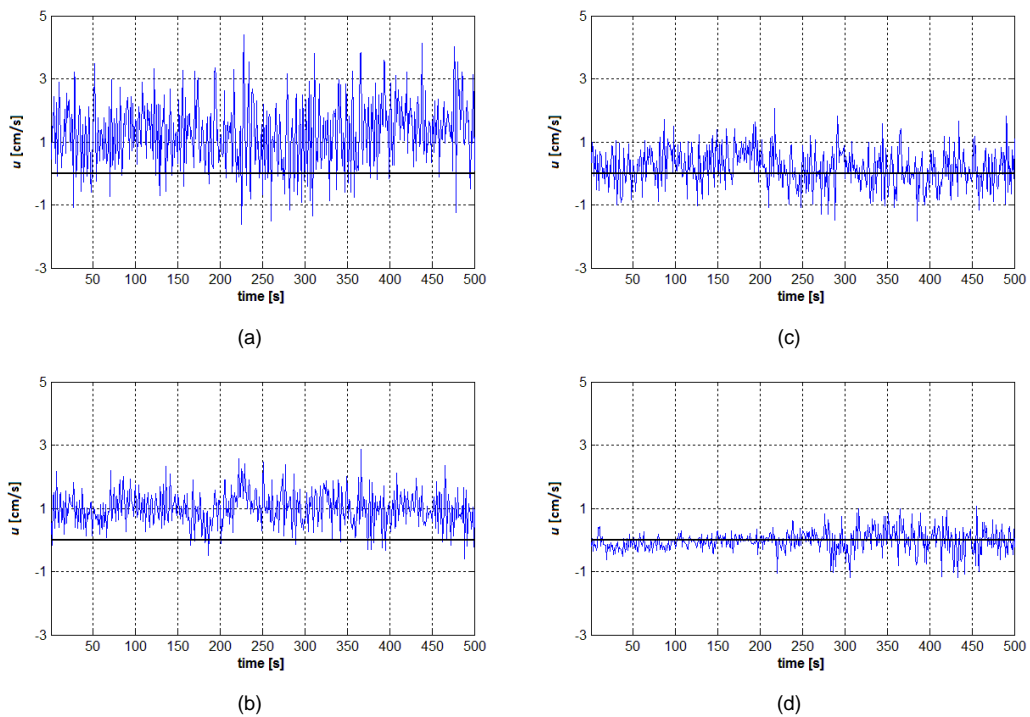


**Fig. 2.** Time series of the instantaneous perpendicular velocity component. (a) -8 m and 0.32 m; (b) -8 m and 0.88 m; (c) 0 m and 0.29 m and (d) 0 m and 0.86 m, respectively.

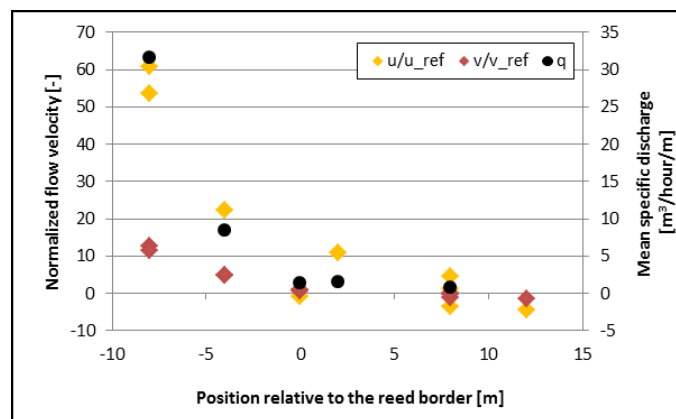


**Fig. 3.** Normalized perpendicular and parallel flow velocity and mean specific discharge versus the position relative to the reed border. Negative positions refer to open water locations and positive ones to locations within the reed zone.

**Tab. 2.** Normalized perpendicular and parallel flow velocity and mean specific discharge through the reed – open water interface zone

distance from the reed border	$u/u_{ref}$	$v/v_{ref}$	$q_{in}$	$q_{out}$	$q$
m	-	-	$m^3/(hour \cdot m)$	$m^3/(hour \cdot m)$	$m^3/(hour \cdot m)$
-8	60.83	12.61	43.70	-12.21	31.62
-4	22.30	4.90	14.68	-6.55	8.37
0	1.00	1.00	17.16	-15.60	1.39
2	10.80	-0.56	9.75	-8.21	1.52
8	-3.52	-1.07	15.63	-14.91	0.69

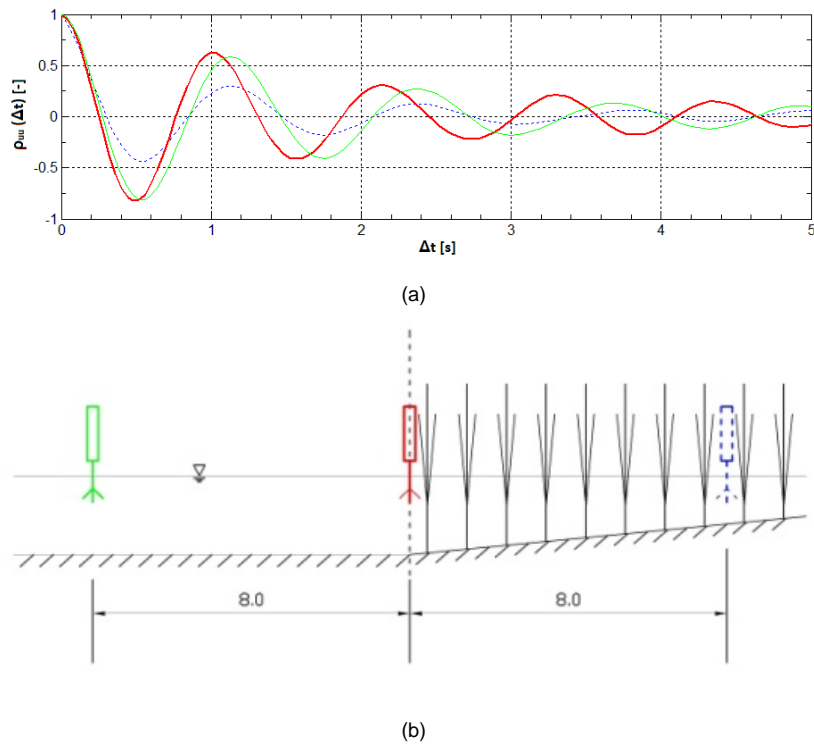


**Fig. 4.** (a) Autocorrelation function of the vertical flow velocity component at three different locations and (b) the measurement locations

nearly equal in the open water and right at the reed border, however, energy decreases rapidly within the canopy suggesting an increased rate of kinetic energy dissipation between the vegetation stems. In fact, the wave-related energy content of the flow within the canopy is almost two orders of magnitude less than that of the open water zone.

#### 4.4 Energy dissipation

The rate of energy dissipation was evaluated in each measurement point with the inertial dissipation method described in Chapter 3.3. The mean and standard deviation of the dissipation rate obtained from velocity component perpendicular to the reed border are plotted in Fig. 6 with dots and error bars. Along this, the dissipation calculated by the theoretical formula Eq. (10) according to [20] is presented with rhombuses. Here, water depth ( $H$ ) and the RMS of the velocity component was applied as the characteristic length and velocity scale, respectively. While in the open water region the theoretical formula approaches the spectrum-based estimates of dissipation rate reasonably well; in the reed zone an underestimation of one to two orders of magnitude was observed. Presumably, the reason lies in the diverse way of turbulent production in emergent vegetation. Within the reed stems, the production of turbulence through bed shear becomes negligible compared to the production within stem wakes, except a thin layer very close to the bed [15]. Thus the kinetic energy budget can be reduced to the balance of wake production and energy dissipation. In this case, however, the characteristic length scale of the turbulence is not any more given by the water depth but rather by the average stem diameter ( $d$ ) as it was suggested by [16]. In fact, the estimated dissipation rate based on the scale assumption  $L \sim d$ , indicated by triangles in Fig. 6, is in a good agreement with the spectrum-based estimation.

#### 4.5 Decomposition aspects and outcome of the turbulent components

Turbulent characteristics (such as TKE, shear stress and friction velocity) can be calculated from the turbulent fluctuation of the flow velocity components ( $u'$ ,  $v'$  and  $w'$ ) as described in Chapter 3.4. The turbulent fluctuation term is most frequently determined by means of Reynolds decomposition (RD) which gives the turbulent fluctuation by subtracting the Reynolds averaged mean velocities from the instantaneous velocity components as was presented in Chapter 3.2. In lake environments, however, where waves have a significant contribution to the flow and the energy of waves appear in the total flow energy, calculating the turbulent fluctuation term via RD without further separation of the wave related components from pure turbulence might lead to an inaccurate description of the turbulent characteristics. To investigate the degree of this inaccuracy, RD and a second procedure (referred hereafter as WD) which enables decomposition of wave related components from turbulent components were applied on the same data series. Furthermore, the turbulent

characteristics gained via the two descriptions were compared to each other.

The detailed description of WD can be found in [7], in the following only its main idea will be presented. First, high pass filtering is used to remove the components of longer time scale (e.g. seiche, circulatory motion or Stokes-drift) yielding time series containing only wave and turbulent components. Note that in case of quasi steady flow, which criteria is fulfilled by the investigated time series, the high pass filtering is basically equivalent with the subtraction of the Reynolds averaged mean. As a next step of WD, the spectrum of the wave and turbulence related velocity components are separated in the frequency domain. Finally, returning from the frequency domain to the time series domain, the time series of the orbital velocity components are calculated by inverse discrete Fourier transformation (DFT).

Fig. 7 demonstrates the role of decomposition of wave related components from turbulent components through the example of one of the investigated time series. The plot shows together the turbulent fluctuation time series obtained via RD (thick line) and WD (thin line). The turbulent fluctuation term derived via RD is on average one order of magnitude larger than the one derived via WD. It is also clearly visible that after RD the remaining time series still contains a regular periodic wave component showing characteristics different from the ones expected from the pure turbulent fluctuation. The presented difference might be important regarding the turbulent kinetic energy budget, the magnitude and the variation of the friction velocity and shear stress at the sediment surface and thus the resuspension potential of the sediment. In addition, if the effect of turbulence on aquatic species (such as phytoplankton, zooplankton or fish) is intended to evaluate (see e. g. [1]), considering the turbulent fluctuation from RD or WD might lead to relevant differences since the sensitivity of the species against the impact of turbulence depends mainly on the characteristic length scale of the eddies and the destruction effect of shear stress.

Several data series were used to investigate the difference between the turbulent characteristics gained via the two procedures and the effect of wind and wave conditions, measurement locations (sheltered or wave exposed) and measurement depths. To extend the investigation in such a way, not only the flow data set presented in Chapter 2 and analysed in the previous sections was used but additional flow data recordings were also involved in the analysis. The main characteristics of the four applied data sets are summarized in Table 3. Two of them (Fertő 2009 lower and Fertő 2009 upper) were recorded near the eastern shore of the lake more exposed to the observed NNW wind as it appears in higher average wave height of Table 3. The notation lower and upper refer to two measurement depth (1.2 and 0.4) of the same vertical. The data set labelled as Fertő 2012 originates from the measurement campaign presented above, when the ADV sensor was located in the immediate vicinity of the reed zone and moderate wind speed, low flow velocities and small wave heights were observed. Finally, a data set recorded in the

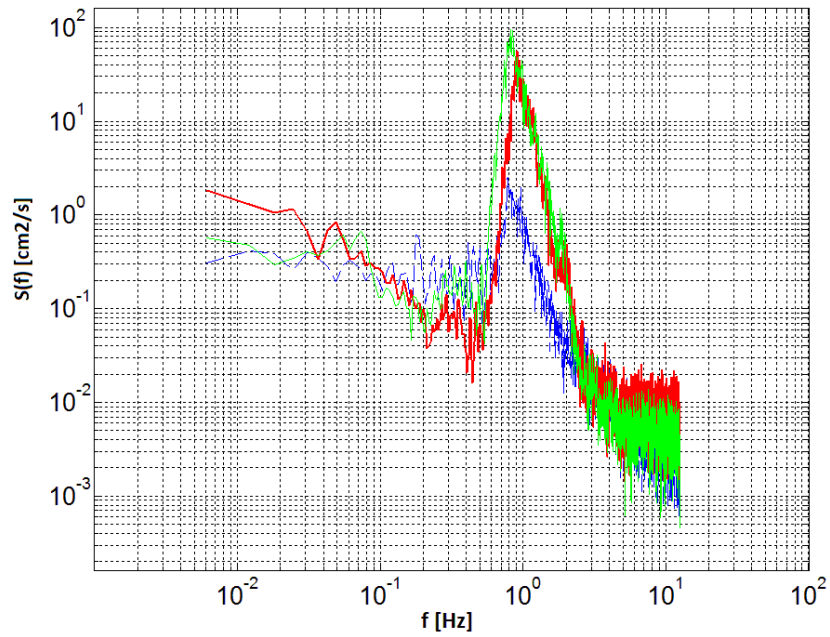


Fig. 5. Power density spectra of the vertical flow velocity component at three different locations (for measurement locations see Fig. 4 (b))

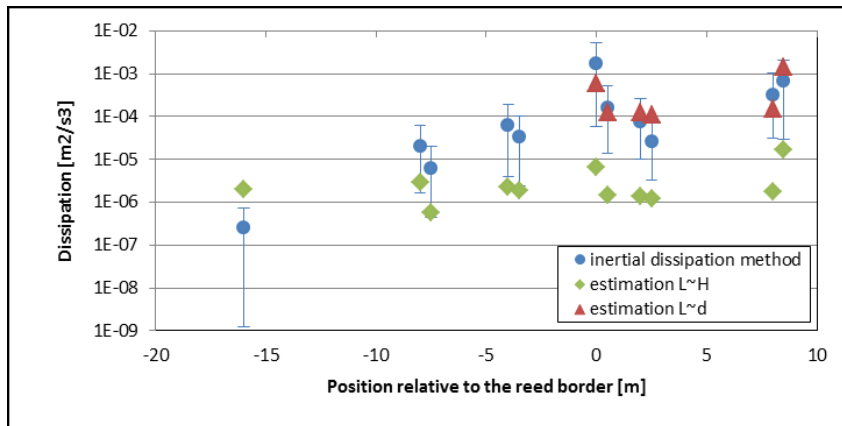


Fig. 6. Energy dissipation rate derived from the inertial dissipation method reed border and the theoretical formula according to [20] versus the position relative to the

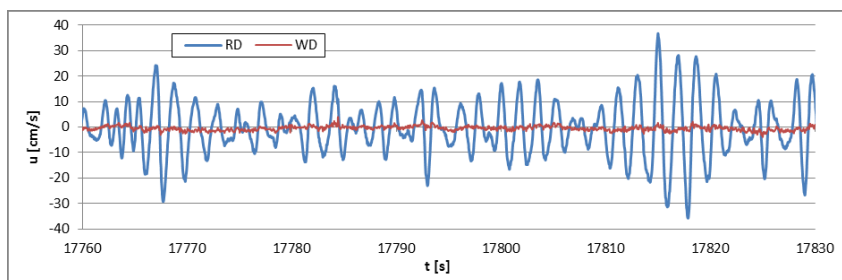
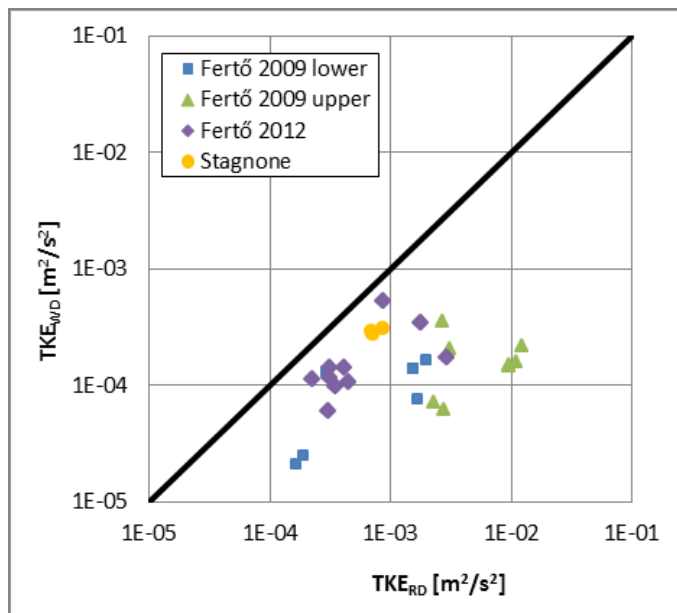


Fig. 7. An example of turbulent fluctuation time series derived via RD (thick line) and WD (thin line)

Stagnone di Marsala lagoon of Sicily (referred as Stagnone) was also studied with its high wind speed but comparatively small waves. All data sets contain 8-minute long recordings of 3D flow velocity data series.

Turbulent kinetic energy, shear stress and friction velocity were calculated from the turbulent time series of both procedures. Since shear stress is given by the turbulent kinetic energy multiplied by a constant according to (10) and the relationship of (11) exists between friction velocity and shear stress, only the most representative TKE was chosen for presentation.

In Fig. 8, TKE of turbulent time series gained via WD and RD are plotted against each other. The four data sets are marked differently. Different degree of discrepancy can be observed from the thick line representing the line of perfect agreement between the two procedures. In case of the minimal discrepancy, which characterises some of the time series of Fertő 2012 and Stagnone,  $TKE_{RD}$  is twice as large as  $TKE_{WD}$ . The common feature of these recordings is the low average wave height presumably due to the sheltered location from the wind. The ratio of  $TKE_{RD}$  and  $TKE_{WD}$  is significantly higher considering the time series of data sets of the wind and wave exposed Fertő 2009 lower and Fertő 2009 upper points. As a maximum, the ratio reaches an extremely high value of nearly 70 in the upper measurement point of Fertő 2009 campaign when rather strong wind of 7.1 m/s arrived exceeding the average wind speed of the data set and as a consequence high waves with about 18 cm developed.



**Fig. 8.** Turbulent kinetic energy estimated from turbulent time series gained via Reynolds decomposition (RD) and wave decomposition (WD) procedures.

These calculations confirm that in a lake environment turbulent estimation based on turbulent fluctuation time series derived from Reynolds decomposition can be inaccurate even with some orders of magnitude, and the rate of inaccuracy rises with the magnitude of wave-related energy content of the flow. Consequently, in cases when precise estimation of turbulent character-

istics is needed or when waves are significant, the use of a more sophisticated decomposition procedure is suggested to separate the wave related components from turbulent components.

#### 4.6 Turbulent characteristics and sediment resuspension

According to the previous chapter, the turbulent fluctuation time series derived from the decomposition procedure after [7] was applied to estimate the turbulent characteristics near and inside the reed canopy. The parameters of Table 4 characterise the near-bed structure of turbulence, resuspension and deposition of sediment at each measurement location.

Reynolds number of the open water zone decreases with decreasing distance from the reed border, which is in agreement with [12]. Within the reed zone  $Re$  reaches a nearly constant value which is lower than the ones of open water zone. As critical Reynolds number is between 600 and 12500 [9], the fully turbulent flow at the open water locations becomes transient within the canopy, indicating that flow inside the reed zone is neither fully turbulent nor fully laminar.

Along  $Re$ , the stem diameter based Reynolds number ( $Re_d$ ) of the reed zone is also presented in Table 4.  $Re_d$  characterises the wake structure and describes how the wake affects the turbulent kinetic energy and diffusion within the array of canopy stems. The transition from laminar to turbulent wake structure was investigated by [21] focusing on an isolated cylinder in a uniform flow. The critical  $Re_d$  was found to be about 200 above which the wake becomes turbulent due to the vortex instability; however vortex shedding was shown to initiate at lower  $Re_d$  of about 50. Among others, [15] demonstrated that within a cylinder array the vortex shedding delays in consequence of the lateral shear of the upstream wakes and it occurs at higher  $Re_d$  of 150 to 200. In addition, the dependence of the delay on the array density was also presented. According to these studies, the flow within the reed canopy in our experiment can be regarded to fall into the laminar range, since  $Re_d$  is in the order of 100 at each measurement points of the reed zone.

In the following, two simple procedures will be presented to evaluate the sediment deposition and resuspension potential in the interface zone. Both procedures are based almost solely on velocity measurements denoting the wide applicability of these estimations.

Considering the suspended sediment concentration (SSC) with its mean value of 70 mg/l measured between 1992 and 2006 in the lake in similar conditions, the sediment deposition can be estimated as the product of this mean SSC and the specific discharge derived in Chapter 4.2. Currents entering the reed zone rapidly slow down (see Chapter 4.1) and penetrating waves quickly attenuate indicated by the decrease of the wave-related energy content (see Chapter 4.3). As a consequence, sediment stirring up capability drops and deposition becomes dominant. Therefore, the assumption can be made that at last all incoming suspended sediment tends to deposit. The specific sediment deposition ( $SD_{in}$ ) estimated in such a way taking into account

**Tab. 3.** The main features of data sets applied in the investigation of decomposition procedures prior to turbulent characteristic estimation

	GPS coordinates - East	GPS coordinates - North	avg wind speed	avg wave height	water depth	meas. depth
			m/s	cm	m	m
Fertő 2009 lower	E 16°44'36.6"	N 47°46'16.5"	5.9	13.2	1.6	1.2
Fertő 2009 upper	E 16°44'36.6"	N 47°46'16.5"	5.9	14.6	1.6	0.4
Fertő 2012	E 16°43'32.2"	N 47°42'51.1"	1.7	3.5	0.7	0.2
Stagnone	E 12°27'9.3"	N 37°52'16.5"	7.3	5.3	1.25	0.6

**Tab. 4.** Parameters of the turbulent characteristics and sediment resuspension near and inside the reed canopy

distance from reed border	relative depth	wind speed	wind direction	$Re$	$Re_d$	$TKE$	$\tau$	$u_{b*}$	$TI$
m	m/m	m/s		-	-	$m^2/s^2$	$N/m^2$	m/s	-
-16	0.28	1.0	SE	29191	-	6.94E-04	1.32E-04	3.63E-04	0.72
-8	0.32	2.4	SE	16106	-	2.96E-03	5.62E-04	7.50E-04	1.96
-8	0.88	2.7	SE			3.07E-04	5.83E-05	2.42E-04	0.89
-4	0.26	1.3	NE	10204	-	4.14E-04	7.88E-05	2.81E-04	1.33
-4	0.71	0.7	N			3.09E-04	5.86E-05	2.42E-04	1.34
0	0.29	2.3	SE	4834	69	1.77E-03	3.36E-04	5.80E-04	4.55
0	0.86	2.1	SE			3.09E-04	5.88E-05	2.42E-04	3.82
2	0.31	1.5	N	8317	119	4.52E-04	8.59E-05	2.93E-04	1.75
2	0.74	1.6	NE			3.49E-04	6.64E-05	2.58E-04	1.60
8	0.36	1.5	N	6701	96	2.27E-04	4.31E-05	2.08E-04	2.05
8	0.74	1.1	N			8.74E-04	1.66E-04	4.08E-04	2.49

only the incoming specific discharge was 29 kg/day/m right at the reed border. However, the specific sediment deposition ( $SD$ ) derived from the mean specific discharge considering both the incoming and outgoing specific discharge was 2.6 kg/day/m. In general, it can be stated that under wind and flow conditions similar to the ones of the investigation period, the specific sediment deposition might be close to the estimated  $SD_{in}$  value and most likely it tends to fall into the interval given by  $SD$  and  $SD_{in}$ .

Since erosion and thus resuspension can only occur when the drag and lifting force of the flow exceed the gravitational and friction forces, the sediment resuspension is governed by the near-bed turbulence of the flow [14]. According to [14], resuspension occurs when shear stress at the sediment surface  $\tau$  exceeds the critical shear stress  $\tau_c$ . The latter can be determined by means of the Shields diagram. Applying the average particle size of silt (0.02 - 0.002 mm), the estimated critical shear stress is in the order of  $7E-03 \text{ N/m}^2$ , which is greater than the calculated actual shear stress Eq. (10) at each location (Table 4). The results indicate that presumably no resuspension took place during these investigations neither within the reed zone nor in a short distance from it, which also proves the previous assumption of sediment deposition tendency to be correct. As a good indicator of the sedimentation rate, gradual slight expansion of the reed cover can be observed in the area of our measurement site from year to year, as also seen in Fig. 1. This is the sign of gradual siltation, and as a consequence shallow enough conditions for the reed to expand.

## 5 Conclusions

Lake flow inside and in the immediate vicinity of reed canopies can be assumed as a flow of great complexity since it is induced by the spatially and temporally varying wind field of the reed – open water interface zone, and altered by the abruptly changing morphology of the near-canopy lake bottom and by the enhanced drag of reed stems. The flow field near and inside the reed zone differs in a number of characteristics from the one of the open regions such as flow velocity, wave and turbulent characteristics, energy budget, etc. Though several types of current meters are available for researchers, most of them are not adaptable for measurements inside the canopy of low water depth and densely standing plant stems. Probably, this is one of the reasons for the insufficiently revealed flow features near and inside these canopies. However, the exploration of the quite complex flow field near and inside the canopy has got a great importance, since the exchange mechanisms playing a crucial role in the quality of the reed water, thus the biodiversity of reed zones are controlled primarily by these near-canopy flow conditions.

The present work intended to enhance the understanding of the gradient-driven interactions and exchange mechanisms of the reed – open water interface. 3D flow velocities along one interface zone of Lake Fertő were investigated. With two synchronised Nortek Vectrino Lab Probes high frequency (25 Hz)

recordings were conducted in multiple locations from 16 m outside the reed zone to 12 m inside at two depths of each vertical. Furthermore, the flow field, specific discharge, energy dissipation rate, turbulent characteristics and sediment deposition and resuspension tendency were analysed and parameterised near and inside the reed zone.

The reduction of mean perpendicular velocity and velocity fluctuation was revealed moving toward the vegetation and toward the lake bottom. Similarly, considering the velocity components normalized by the reference point measurement to account for unsteady conditions, an exponential reduction could be observed moving towards and into the reed zone. At some inner locations, perpendicular velocities of the same vertical directed opposite to each other at different depths, indicating a return flow within the canopy. This suggests that near and within the canopy 3D description of the flow structure is needed.

The power density spectra of the vertical velocity components proved the rapid decrease of wave-related energy moving inside the reed zone. At 8 m inside the canopy the wave-related energy content of the flow was almost two orders of magnitude less than that of the open water zone.

The rate of energy dissipation, which was evaluated with the inertial dissipation method from the calculated power spectral density of the perpendicular velocity components, showed an increasing tendency moving toward and into the vegetation. It was also presented that the theoretical formula for energy dissipation estimations introduced by [20] approximated better the calculated dissipation rate within the reed zone if the average stem diameter was considered as the characteristic length scale of the turbulence instead of the average water depth. This confirmed the assumption of [15] that within the reed stems the production of turbulence through bed shear becomes negligible compared to the production within stem wakes, thus the kinetic energy budget can be reduced to the balance of wake production and energy dissipation.

To characterise the near-bed structure of turbulence and the resuspension as well as deposition of sediment in the investigation area, the turbulent characteristics were estimated. As a first step, however, the effect of different decomposition techniques on the turbulent characteristics was investigated. It was found that turbulent characteristics calculated via Reynolds decomposition (RD) might exceed significantly the ones derived via a technique according to [7] which enables the decomposition of wave related components from turbulent components (referred to in this paper as WD). As an example, turbulent kinetic energy via RD was from twice to nearly 70 times as large as the one via WD depending remarkably on the magnitude of the wave-related components. According to this, the conclusion was drawn that in cases when precise estimation of turbulent characteristics is needed or when waves are significant, the decomposition of wave-related components from turbulent components is suggested. Based on this this consideration, the turbulent characteristics were estimated via WD at each measurement points.

Considering the Reynolds number in general and the critical one given by [9], the flow was fully turbulent at the open water locations and transient within the canopy. According to another estimation, however, which lies on the stem diameter based Reynolds number, the flow within the reed zone was rather laminar. Regarding the sediment deposition and resuspension potential, two estimation procedures confirmed the tendency for continuous sediment deposition and the lack of resuspension in the investigated area near and inside the reed zone. The presented results characterise well the most frequent processes taking place at the reed – open water interface since general wind and flow conditions of the lake were observed during the measurement campaign with moderate wind velocities and flow velocities not exceeding 3 cm/s at that site. Note, however, that measurements at higher current velocities are needed for more detailed investigations and for revealing the flow velocity and the distance from reed border where sediment resuspension starts to dominate.

## References

- 1 **Baranyai E, G.-Tóth L, Vári Á, Homonnay Z G.** *The effect of variable turbulent intensities on the distribution of zooplankton in the shallow, large Lake Balaton (Hungary)*, Knowledge and Management of Aquatic Ecosystems, **400**, (2011), DOI 10.1051/kmae/2011003.
- 2 **Bengtsson L, Hellström T.** *Wind-induced resuspension in a small shallow lake*, Hydrobiologia, **241**(3), (1992), 163–172, DOI 10.1007/BF00028639.
- 3 **Cea L, Puertas J, Pena L.** *Velocity measurements on highly turbulent free surface flow using ADV*, Experiments in Fluids, **42**(3), (2007), 333–348, DOI 10.1007/s00348-006-0237-3.
- 4 **Clarke S J.** *Aquatic Plants*, *Encyclopedia of Lakes and Reservoirs*, 2012, ISBN 978-1-4020-5616-1 (Print), 978-1-4020-4410-6 (Online).
- 5 **Emery W J, Thomson E.** *Data Analysis Methods in Physical Oceanography*, 2nd Edition, Elsevier Science, 2001.
- 6 **Fukuhara H, Nemoto F, Takeuchi Y, Toda N.** *Nitrate dynamics in a reed belt of a shallow sand dune lake in Japan: Analysis of nitrate retention using stable nitrogen isotope ratios*, Hydrobiologia, **584**(1), (2007), 49–58, DOI 10.1007/s10750-007-0589-6.
- 7 **Homoródi K, Józsa J, Krámer T, Ciraolo G, Nasello C.** *Identifying wave and turbulence components in wind-driven shallow basins*, Periodica Polytechnica Civil Engineering, **56**(1), (2012), 87–95, DOI 10.3311/pp.ci.2012-1.10.
- 8 **Horppila J, Nurminen L.** *Effects of different macrophyte growth forms on sediment and P resuspension in a shallow lake*, Hydrobiologia, **545**(1), (2005), 167–175, DOI 10.1007/s10750-005-2677-9.
- 9 **Kadlec R H.** *Overland Flow in Wetlands: Vegetation Resistance*, Journal of Hydraulic Engineering, **116**(5), (1990), 691–706, DOI 10.1061/(ASCE)0733-9429(1990)116:5(691).
- 10 **Kim S-C, Friedrichs C T, Maa J P, Wright L D.** *Estimating Bottom Stress in Tidal Boundary Layer from Acoustic Doppler Velocimeter Data*, Journal of Hydraulic Engineering, **126**(6), (2000), 399–406, DOI 10.1061/(ASCE)0733-9429(2000)126:6(399).
- 11 **Kiss M, Józsa J.** *Wind profile and shear stress at reed-open water interface: recent research achievements in Lake Fertő*, Pollack Periodica, (2014). in press.
- 12 **Leonard L A, Luther M E.** *Flow hydrodynamics in tidal marsh canopies*, Limnology and Oceanography, **40**(8), (1995), 1474–1484, DOI 10.4319/lo.1995.40.8.1474.
- 13 **Madsen J D, Chambers P A, James W F, Koch E W, Westlake D F.** *The interaction between water movement, sediment dynamics and submersed macrophytes*, Hydrobiologia, **444**(1-3), (2001), 71–84, DOI 10.1023/A:1017520800568.
- 14 **Middleton G V, Southard J B.** *Mechanics of Sediment Movement*, Soc. Econ. Paleontol. Mineral., 1984, DOI 10.2110/scn.84.03.
- 15 **Nepf H M, Sullivan J A, Zavistoski R A.** *A model for diffusion within emergent vegetation*, Limnology and Oceanography, **42**(8), (1997), 1735–1745.
- 16 **Nepf H M.** *Drag, turbulence, and diffusion in flow through emergent vegetation*, Water Resources Research, **35**(2), (1999), 479–489, DOI 10.1029/1998WR900069.
- 17 **Pannonhalmi M, Sütthő L.** *A Fertő tó múltja, jelene és jövője [In Hungarian: Past, present and future of Lake Fertő]*, ÉDUKÖVIZIG, 2007.
- 18 **Pope S B.** *Turbulent Flows*, Cambridge University Press, 2000, DOI 10.1017/CBO9780511840531.
- 19 **Soulsby R L, Dyer K R.** *The form of the near-bed velocity profile in a tidally accelerating flow*, Journal of Geophysical Research, **86**(C9), (1981), 8067–8074, DOI 10.1029/JC086iC09p08067.
- 20 **Tennekes H, Lumley J L.** *A First Course in Turbulence*, MIT Press, 1972.
- 21 **Williamson C H K.** *The natural and forced formation of spot-like ‘vortex dislocations’ in the transition of a wake*, Journal of Fluid Mechanics, **243**(1), (1992), 393–441, DOI 10.1017/S0022112092002763.
- 22 **Zhang X, Nepf H M.** *Thermally driven exchange flow between open water and an aquatic canopy*, Journal of Fluid Mechanics, **632**, (2009), 227–243, DOI 10.1017/S0022112009006491.